Delft University of Technology

Microstructure, surface chemistry and electrochemical response of Ag|AgCl sensors in alkaline media

Pargar, Farhad; Kolev, H; Koleva, Dessi; van Breugel, Klaas

Important note
To cite this publication, please use the final published version (if applicable).
Please check the document version above.

CrossMark

Microstructure, surface chemistry and electrochemical response of Ag|AgCl sensors in alkaline media

Farhad Pargar[1,*] ⓘ, Hristo Kolev[2] ⓘ, Dessi A. Koleva[1] ⓘ, and Klaas van Breugel[1] ⓘ

[1] Faculty of Civil Engineering and Geosciences, Materials and Environment, Technische Universiteit Delft, Stevinweg 1, 2628 CN Delft, The Netherlands
[2] Institute of Catalysis, Bulgarian Academy of Sciences, Acad. G. Bonchev Str., bl. 11, 1113 Sofia, Bulgaria

ABSTRACT

Characterization of the Ag/AgCl electrode is a necessary step toward its application as a chloride sensor in a highly alkaline medium, such as concrete. The nucleation and growth of AgCl on Ag in 0.1 M HCl was verified through cyclic voltammetry. Ag anodization was performed at current densities, determined by potentiodynamic polarization in the same (0.1 M HCl) medium. The morphology and microstructure of the AgCl layers were evaluated via electron microscopy, while surface chemistry was studied through energy-dispersive spectroscopy and X-ray photoelectron spectroscopy. At current density above 2 mA/cm^2, the thickness and heterogeneity of the AgCl layer increased. In this condition, small AgCl particles formed in the immediate vicinity of the Ag substrate, subsequently weakening the bond strength of the Ag/AgCl interface. Silver oxide-based or carbon-based impurities were present on the surface of the sensor in amounts proportional to the thickness and heterogeneity of the AgCl layer. It is concluded that a well-defined link exists between the properties of the AgCl layer, the applied current density and the recorded overpotential during Ag anodization. The results can be used as a recommendation for preparation of chloride sensors with stable performance in cementitious materials.

Introduction

The determination of the chloride content in reinforced concrete (RC) structures is important for the assessment of the probability of chloride-induced corrosion of steel reinforcement. Although the application of Ag/AgCl sensors for the above purpose is well known, the benefits and drawbacks of utilization of these sensors are still a subject of discussion [1–3]. Discussions concern the OCP responses of the sensors in alkaline medium and the observed scatter among these responses. For instance, similar Ag/AgCl sensors are reported to give a different response to identical alkaline medium, which is a nonexpected outcome. While the sensor's response is just a common open-circuit potential (OCP) record, i.e., the Ag/AgCl electrode potential reading, the possible discrepancies will reflect the

Address correspondence to E-mail: F.Pargar@tudelft.nl

time needed for establishing a dynamic equilibrium at the sensor/environment interface. Although fundamental electrochemical thermodynamics and kinetics can explain these discrepancies [4–12], practical application of the Ag/AgCl sensors for RC structures is still to be justified. This justification refers to specifying the limits for these sensors' application and the reasons behind the existence of such limits.

The motivation of this work lies in an attempt to clarify the origin of the unexpected results obtained with Ag/AgCl sensors in alkaline medium. The lack of agreement among the OCP response of the sensors has been reported as partly attributable to the sensors' preparation methods [1]. Varying physical properties of the AgCl layer were considered as the reason for OCP responses, different from those expected [2]. The potentially weak bond between the AgCl layer and the Ag substrate of the sensor, a bond which develops during sensor's preparation, has been suggested as the main reason for the poor performance of the sensor in alkaline medium [3], although this has not been experimentally justified. Hence, the experimental evidence to support this hypothesis is scarce [1, 4].

The thermodynamic considerations and the kinetics of AgCl formation on a Ag substrate were subject to numerous works in the fields of electrochemistry and crystal growth since the early 1950s [5–11]. Despite the results in these thoroughly elaborated works, the properties and performance of Ag/AgCl electrodes in the alkaline medium are yet to be affirmed, especially in view of their application as chloride sensors for RC structures.

One of the reasons for a limited number of reports on the correlation between the properties of the AgCl layer and the response of the sensor in alkaline medium is related to unsuccessful attempts for observing the inner morphology of the AgCl layer. For instance, as reported in [4, 11, 12]: microscopic observations of the Ag/AgCl interface was problematic. The attempts to stiffen the sample by Cu and Ni–P plating or liquid N_2 (low temperature of approx. − 190 °C) was not successful, since the soft AgCl particles would spread over the entire surface of the samples and mask the interface. Sample preparation to address the above challenges is discussed in this work and is part of in-depth investigation of the Ag/AgCl sensors' performance in alkaline medium.

Different techniques are available for the AgCl formation on a Ag substrate [13]. The AgCl layer can be attached (physically bond) on the Ag substrate by dipping Ag in molten silver chloride, the layer can be electrochemically formed by anodization in HCl solution, or chemically formed, by oxidation with aqueous $FeCl_3$ solution. The choice of a technique is determined by a general attempt to improve the performance of Ag/AgCl electrodes in view of their sensitivity to various parameters, involved in the manufacturing process. For instance, in the case of screen printing, a Ag–AgCl paste is deposited on a metallic surface (e.g., Pt) to produce the Ag/AgCl electrode. The adhesive properties of the paste to the supporting electrode might not be very good; hence, the reliability of the sensor will depend on the homogeneity of the Ag–AgCl paste used [14]. In general, the relatively small contact area, i.e., weak adhesion between the Ag rod and AgCl layer, may lead to oxidation of AgCl at Ag/AgCl interface by hydroxide ions from the alkaline medium at a relatively fast rate [15].

One of the most frequently used methods for Ag/AgCl sensor preparation is anodization of Ag in a HCl solution [16–19]. The low pH of a HCl solution would limit the possible Ag_2O formation [20, 21] and would result in AgCl formation on the Ag substrate. A layer of AgCl with sufficient thickness was considered to be of ca. tens of the micrometer range [12]. With anodization, the rate of AgCl formation depends on the applied current density and the time of the anodization [22]. Different current density and anodizing time have been reported for the preparation of sensors, e.g., 0.4 mA/cm^2 for 30 min [16, 19], 2 mA/cm^2 for 30 min [17], 0.2 mA/cm^2 for 1 h [18], 0.4 mA/cm^2 for 2 h [3]. Logically, as with each electrochemical process of this kind, the anodization regime will affect the produced layer thickness, surface morphology and ionic/electron conductivity, respectively [5, 10]. These features of the AgCl layer may subsequently be reflected in the electrochemical response of the sensor [20], especially in alkaline medium. For instance, a porous microstructure of the AgCl layer increases the probability of a mixed potential by limiting the rate at which the sensor can achieve equilibrium potential [23]. This should be avoided, if possible, in order to achieve a more accurate and reliable sensor's response.

Considering aforementioned, the focus of this paper is to correlate the properties of the AgCl layer to the anodization regime and link these to the actual electrochemical response of the sensor in chloride-

containing alkaline medium. The importance of this correlation is in view of the research question: how different morphology, microstructure and composition of the AgCl layer are important for the accuracy of a sensor and determination of the chloride content in a relevant medium. The significance of the above dependencies is also evaluated in view of the intrinsic conductivity of a AgCl layer (ionic and electron conductivity), more importantly how these properties determine an electrochemical equilibrium at a sensor/solution interface, i.e., the sensor's response, is also addressed.

Experimental materials, methods and technical background

Electrochemical tests on Ag in 0.1 M HCl

Linear sweep cyclic voltammetry (CV) and potentiodynamic polarization (PDP) were employed as screening techniques to derive information for AgCl formation on the Ag substrate. Ag wires of 99.5% purity, 1 mm diameter, were supplied by Salomon's Metalen B.V. Netherlands. The CV and PDP tests were carried out in 0.1 M HCl solution (pH $\sim$ 1.4) in a conventional three-electrode cell arrangement, where the Ag wire (1 cm length) was the working electrode, a Pt mesh was the counter electrode and a saturated calomel electrode (SCE) was the reference electrode. The CV scans were performed from -400 to $+150$ mV (versus OCP) at a scan rate of 100 mV/s with the aim to verify AgCl nucleation and growth in the chosen medium. PDP was performed in the range of -200 to $+1600$ mV versus OCP at a scan rate of 0.5 mV/s. The PDP test results determined the range of current densities, potentially suitable for anodizing Ag in the chosen medium. The CV and PDP tests were performed using PGSTAT 302N potentiostat (Metrohm Autolab B.V., The Netherlands).

Ag anodization: preparation of Ag/AgCl sensors

The Ag wires were cleaned for 2 h in concentrated ammonia, then immersed in demineralized water overnight, prior to anodization in 0.1 M HCl solution. Anodization was carried out in two manners: (1) at 4 mA/cm^2 with varying anodization time from 900 s

to 1 h, and (2) for equal duration of 1 h, but at four different current densities, i.e., 0.5 mA/cm^2 (regime A), 1 mA/cm^2 (regime B), 2 mA/cm^2 (regime C) and 4 mA/cm^2 (regime D). The wires anodized in the first manner, i.e., highest current density and varying time of anodization, are designated as D-type sensors, since they formed a parallel group of the D sensors, prepared via the second approach at 4 mA/cm^2 for 1 h anodization only. The D-type sensors were only used for microscopic investigations of the Ag/AgCl interface and as supportive evidence to the results for all other sensor types, including the discussion on ohmic resistance of the AgCl layers. The experimental setup and instrumentation for sensors' preparation were identical to the one for the CV and PDP tests. The current regimes were chosen based on the PDP screening test as specified in "Electrochemical tests on Ag in 0.1 M HCl" section. The thickness of the AgCl layer was both experimentally determined ("Morphology, microstructure and surface chemistry of the AgCl layer" section) and theoretically approximated by employing Eq. (1), which essentially is a modification of Faraday's law:

$$X = \frac{i \cdot M \cdot t}{F \cdot d} \tag{1}$$

where X is the thickness of the AgCl layer (cm); i is the applied current density (A/cm^2); M is the molecular weight of AgCl, 143.5 g/mol; t is the duration of anodization; F is the Faraday's constant ($F = 96500$ C/mol/equiv); d is the density of the AgCl layer, 5.56 g/cm^3. The theoretical approximation of a AgCl layer after Ag anodization is also reported in the literature [5].

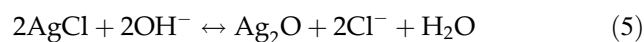### Ag/AgCl sensors' response in alkaline medium

The sensors' response in a model alkaline medium is their open-circuit potential (OCP) over time. A brief background on OCP-related theory in view of the Ag/AgCl electrode (or sensor) is as follows: recording the OCP of the sensor reflects the main concept of defining the chloride content at the sensor/medium interface. Well known is that Ag/AgCl sensors are predominantly sensitive to chloride ions; hence, their response in chloride-containing medium is directly related to the activity (concentration, respectively) of the chloride ions. This relationship is governed by the Nernst equation (Eq. 2):

$$E = E_{Ag/AgCl}^0 - 2.303 \frac{RT}{nF} \lg[a_{Cl^-}] \tag{2}$$

where E is the measured OCP of the sensor versus a reference electrode such as SCE, $E_{Ag/AgCl}^0$ is the standard electrode potential for the Ag/AgCl electrode (V), a_{cl^-} is the activity of the chloride ions (mol dm^{-3}) in the vicinity of the electrode, R is the gas constant (J mol^{-1} K^{-1}), F is the Faraday constant (C mol^{-1}) and T is the absolute temperature (K). The chloride ions concentration (C_{Cl^-}) [molality] can be calculated further, using the relationship in Eq. (3), employing the activity coefficient γ_{cl^-} [24].

$$a_{cl^-} = C_{Cl^-} \cdot \gamma_{Cl^-} \tag{3}$$

Equation (2) is based on the electrochemical exchange equilibrium, presented by Eq. (4), which takes place on the surface of the sensor in chloride-containing medium. In the alkaline medium of zero or low chloride ions content, the adopted OCP will deviate from the one following Eq. (2), since interfering hydroxide ions will dominate the potential response, i.e., E will not present the Ag/AgCl equilibrium only, but also reflect a mixed potential of a Ag/AgCl/Ag$_2$O interface. In this case, the exchange equilibrium presented by Eq. (5) will be relevant.

$$Ag + Cl^- \leftrightarrow AgCl + e^- \tag{4}$$

$$2AgCl + 2OH^- \leftrightarrow Ag_2O + 2Cl^- + H_2O \tag{5}$$

More details on the theoretical aspects of Ag/AgCl response in alkaline medium, and relevant constraints, are reported in a recent review on the subject and references therein [25].

The OCP of the chloride sensors, as produced in different anodization regimes, were recorded in chloride-containing cement extract. OCP was monitored by using the specified in "Electrochemical tests on Ag in 0.1 M HCl" section electrochemical setup. The cement extract (CE) of pH ca. 12.8 was obtained by mixing cement powder (CEM I 42.5N) and demineralized water at the ratio of 1:1. The bottled mixture was rotated for 24 h, followed by filtration for obtaining the extract. The chemical composition of CE is as follows: Ca—201 mg/l; K—3.85 mg/l; Na—1.33 mg/l; Al—4 mg/l and Fe < 1 mg/l. Sodium chloride was added as a solid to the desired concentrations of 20 and 260 mM in the CE (CE is a generally used model medium for electrochemical studies, e.g., for steel [26, 27], since it resembles the pore water of cement-based materials).

Morphology, microstructure and surface chemistry of the AgCl layer

The following procedure sequence (Fig. 1) was employed prior to microscopic observations of the Ag/AgCl interface: (1) a portion of the Ag wire was narrowed prior to anodization; (2) the narrowed portion was stretched from the two sides of the notch; (3) this allowed investigation of a "cross section", i.e., the parallel growth of the AgCl layer on the Ag substrate. The obtained cross section resembled a fracture surface. This enabled the inner morphology of the AgCl layer to be well observed. This procedure and sequence were specifically chosen for the purpose of clear differentiation of the AgCl layers' formation on identically handled Ag substrates, but in conditions of different anodization regime (various current density, "Ag anodization: preparation of Ag/AgCl sensors" section). This approach was chosen as the only suitable one to address the objectives of this work and to overcome the challenges with Ag/AgCl sample preparation for microscopy purposes, as specifically outlined in the introduction section.

The AgCl layers were analyzed, using Environmental Scanning Electron Microscopy (ESEM), Philips-XL30 equipped with an energy-dispersive spectrometer (EDS). The samples were examined under accelerating voltage of 20 kV in high vacuum mode.

The surface chemistry was evaluated through X-ray photoelectron spectroscopy (XPS). The measurements were taken using an ESCALAB MkII (VG Scientific) electron spectrometer at a base pressure in the analysis chamber of 5×10^{-10} mbar using twin anode MgK$_\alpha$/AlK$_\alpha$ X-ray source with excitation energies of 1253.6 and 1486.6 eV, respectively. The XPS spectra were recorded at the total instrumental resolution (as it was measured with the FWHM of Ag3d5/2 photoelectron line) of 1.06 and 1.18 eV for MgK$_\alpha$ and AlK$_\alpha$ excitation sources. The processing of the measured spectra included a subtraction of X-ray satellites and Shirley-type background [28]. The peak positions and peak areas were evaluated by a symmetrical Gaussian–Lorentzian curve fitting. The relative concentrations of various chemical species were determined by normalization of the peak areas to their photoionization cross sections, calculated by Scofield [29].
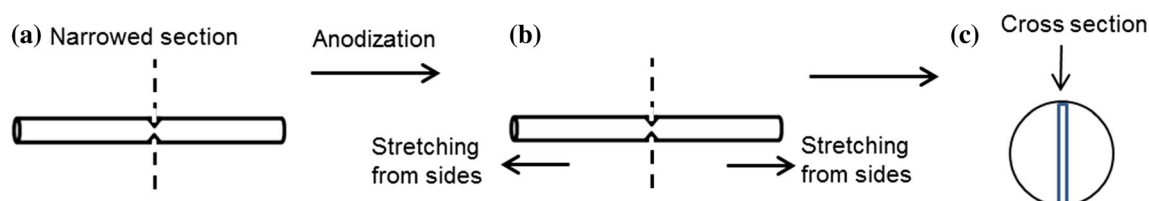
Fig. 1 Procedure sequence for the preparation of a cross section of the Ag/AgCl sensor: **a** narrowing the Ag wire prior to anodization; **b** stretching from both sides after anodization; **c** as a prepared cross section for ESEM observations.

Results and discussion

AgCl nucleation and growth

CV tests

The formation of AgCl on a Ag substrate, from nucleation and growth to reduction and recovery of the AgCl layer in various solutions, has been largely studied over the past decades. Both analytical and experimental works are reported and readily available [7, 9, 30–34]. Studying these processes generally means recording the metal's response to a variety of imposed signals (waves). Linear sweep CV, for example, provides invariable information on the nucleation process, while a PDP response would define the range of current densities for Ag anodization. It is not a subject to this paper to discuss in detail the electrochemistry behind AgCl nucleation and growth, but to rather clarify the chosen approach toward Ag/AgCl sensors preparation. CV and PDP were employed to that end, as screening techniques. Figure 2 depicts CV scans for Ag in 0.1 M HCl, Fig. 2a, and the PDP response in 0.1 M HCl, Fig. 2b.

The aspects of employing CV and the theoretical interpretation of CV scans are reported in detail [35–38] and will be only commented here to the extent of addressing the objectives of this work. When a phase nucleation on a metal surface is involved (as AgCl on Ag), the CV curve (Fig. 2a) will reflect a number of characteristic features: (1) an enhanced anodic and cathodic peak currents separation, which is different from the otherwise observed more narrow response for a general mass transport controlled CV; (2) a characteristic cross-over in the reverse branch of the CV scan will be observed (Fig. 2a, point at $E = 40$ mV); along with (3) the presence of a current maxima in the reversed scan (peak C2 in Fig. 2a), caused by the phase nucleation in the forward scan. The theory and observable characteristic features in a CV scan were formulated

for both interfacial and diffusion control of the crystal growth kinetics [39]. In other words, as seen in Fig. 2a), the hysteresis loop, forming in the reverse scan of the recorded CV for Ag in 0.1 M HCl solution, the cross-over point at ca. 40 mV and the peak C2, define the nucleation of AgCl on the Ag substrate. Next, the cross-over point remains constant with subsequent scans (Fig. 2a, inlet), which proves an interfacial control of the AgCl growth kinetics.

The following features of the CV response (Fig. 2a) can also be noted: practically zero current on the forward scans (also confirming the inertness of Ag in these conditions) was followed by a rapid rise of anodic current, observed at 80 mV in the first scan and 54 mV in the subsequent scans. This single anodic peak (A1) is a Ag dissolution peak in the 1st scan and a stripping peak in the subsequent scans, corresponding to the removal of already formed at negative potentials deposits on the Ag surface. A cathodic shift for the base of the anodic peak was observed with subsequent scans, at the point of the abrupt rise of anodic current (80 mV) (Fig. 2a, inlet). This shift was more significant between the 1st and 2nd CV scans (from 80 to 54 mV), marginal between the 2nd and 5th scans (54–49 mV), and not relevant afterward—toward the 20th scan. Prior to the cathodic current maximum on the reverse scan (peak C2), a nearly linear current–potential region on either side of the cross-over point (at 40 mV) can be observed (Fig. 2a and inlet), where the cross-over potential would equal to the metal–metal ion reversible potential (in this case a slight deviation from the standard potential of 22 mV for the reaction equilibrium at a Ag/Ag^+ interface was observed). The cathodic peak C1 (− 55 mV) was recorded only in the 1st scan and can be associated with: (1) the very first stage of deposition (initiation) of AgCl nuclei [10]; (2) can be due to increased Ag^+ concentration, following the first anodic current increase [40]; (3) and/or can be due to the contribution of an initially smaller size
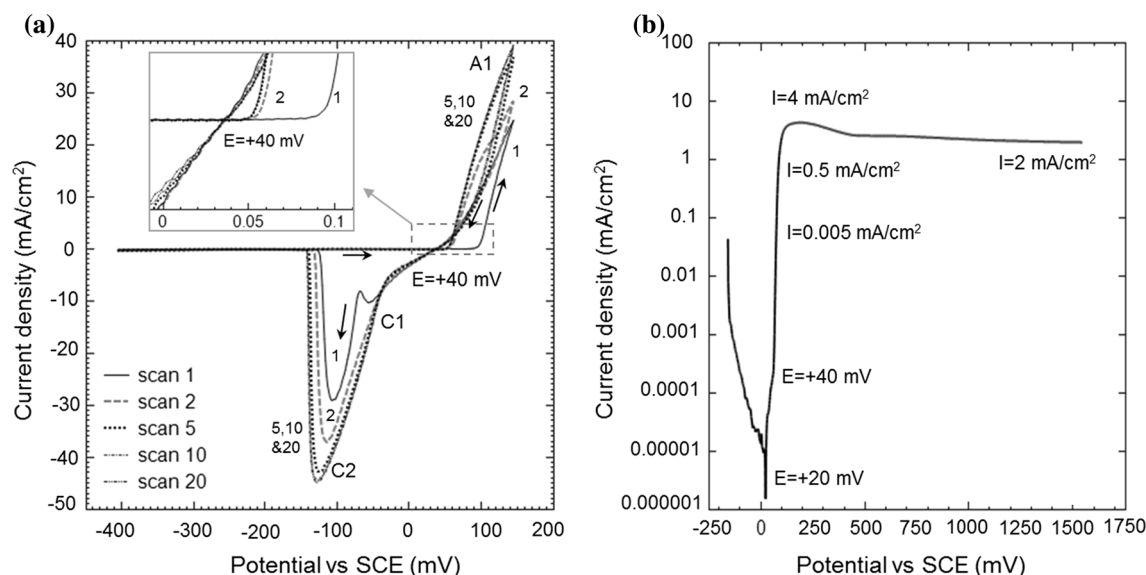
Fig. 2 a An overlay of the 1st, 2nd, 5th, 10th and 20th CV scan for Ag in 0.1 M HCl; **b** PDP curve for Ag in 0.1 M HCl.

AgCl nuclei on the Ag substrate. Similar variation in cathodic peaks potential and currents within AgCl formation on a Ag substrate was reported to be sustained in all scans and linked to the contribution of large (e.g., peak C2) or smaller (e.g., peak C1) AgCl nuclei [10]. However, the mechanism here is obviously different: a reoccurrence of the peak C1 with subsequent scans was not recorded (Fig. 2a). With scanning both anodic and cathodic peaks currents initially increased, Fig. 2a, as expected, while the cross-over point remained at the identical current–potential location, irrespective of the scan number (Fig. 2a and inlet). A constancy of the cross-over point would mean the formation of crystals of a large size, while in contrast, a cathodic shift of this point would be denoted to diffusion-controlled crystal growth and will also imply a decreasing crystal size [39]. A cathodic shift of the cross-over point (Fig. 2a) was not observed. Therefore, the peak C1 most likely reflects an increased Ag^+ concentration during the initial Ag dissolution, followed by initiation of AgCl nuclei formation. The interfacial controlled crystal growth of AgCl nuclei of sufficiently large size is reflected by the shape of the CVs with subsequent scans, where stabilization in both anodic and cathodic currents was observed between the 5th and 20th cycles (Fig. 2a), attributable to the coverage of the Ag substrate by a AgCl layer.

Similar features in a CV response were attributed to a 3D growth of AgCl for Ag/AgCl interfaces in various electrolytes [30, 41, 42]. However, to be noted is that AgCl is known to have a limited electron conductivity, together with a limited ionic conductivity (e.g., for Ag^+ and Cl^- ions, [43]. This will impede a subsequent growth of AgCl on the Ag surface, once a layer of a certain thickness had already developed. As shown in Fig. 2a, the current at anodic and cathodic peaks increases only initially, together with a slight shift of peak potentials (this is between the 1st and the 5th scans). With subsequent scanning no further increase was observed, maintaining the same peaks potential and, as aforementioned, a constant position of the current cross-over point (inlet in Fig. 2a). These features would be consistent with a 2D (rather than 3D) growth process [44], and stabilization of the AgCl layer on the Ag substrate. The actual morphology and microstructure of AgCl, grown on the Ag substrate, will be discussed in detail in "Surface morphology and microstructure" section. The ionic and electron conductivity of the AgCl layer will be discussed in "Correlation of sensors' response, surface properties and ohmic resistance of AgCl" section in relation to the morphological observations.

PDP test

The PDP test was performed to determine the range of suitable current densities for AgCl formation. At potentials more noble than the corrosion potential ($E_{corr} = 20$ mV vs. SCE), the PDP curve shows a sharp increase in anodic current, Fig. 2b. This

increase in current with anodic polarization was almost potential independent until ca. 150 mV, corresponding to an anodic current maximum of 4 mA/cm^2. Stabilization followed after this point and independence of current from potential with further polarization was observed. At potential values more anodic than 300 mV, a limitation of anodic current was relevant with a current stabilization at approx. 2 mA/cm^2. This limitation in the current density can be interpreted as the coverage of the Ag surface by a AgCl layer. Based on the PDP test result (Fig. 2b), the current density range for AgCl layer formation is between ca. 0.05 and 4 mA/cm^2, with 4 mA/cm^2 as a maximum and 0.5–2 mA/cm^2 as an average range, where the Ag substrate is supposedly uniformly covered by AgCl. Therefore, for the Ag anodization process in 0.1 M HCl and Ag/AgCl sensor's preparation, respectively, four current densities in the range of: 0.5–4 mA/cm^2 were employed (regimes A–D in Fig. 3). The current densities of 2 and 4 mA/cm^2 can be referred to as high current densities, while 0.5 and 1 mA/cm^2 are considered as average to low current densities.

The anodization regimes A–D in Fig. 3 are from this point forward used as sensors' designation, i.e., sensors A, B, C and D are discussed in the following sections. Figure 3 also gives the theoretically approximated thickness of the AgCl layer in each regime, together with the experimentally derived one. The former was calculated using the previously introduced Eq. (1); the latter is subject to presentation and discussion in "Surface morphology and microstructure" section.
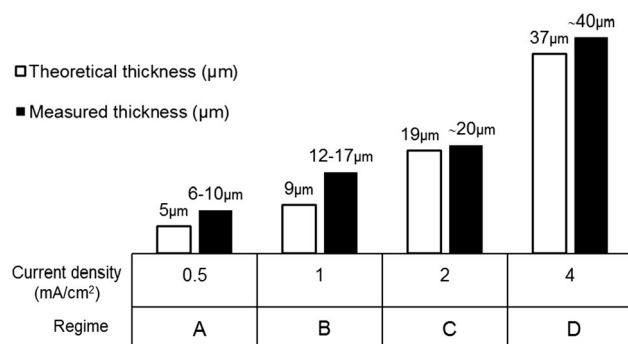
Fig. 3 Anodization regimes for sensor preparation (1-h duration) and thickness of the deposited AgCl layer on the silver substrate.

Sensors' response: OCP records

Background and related general considerations

Evaluating the sensors' response to alkaline medium is important in view of their practical application in a (reinforced) concrete system. In chloride-containing medium the sensors' OCP will return the chloride ions concentration in that medium (in accordance with the previously introduced Eqs. 2, 3 and 4). In the chloride-free environment, as would be in a concrete system where chlorides did not yet penetrate the matrix, the sensors' OCP will reflect a mixed potential and a dynamic exchange equilibrium, similar to Eq. (5), will be relevant. For the former situation, the OCP is expected to shift in cathodic direction and will be determined by the activity of the chloride ions (e.g., for chloride content in the range of 250–500 mM, the OCP value of a chloride sensor should read between 6 and 23 mV vs. SCE [45]). For the latter case, chloride-free alkaline medium, the OCP values are expected to be more anodic (ca. 100–150 mV vs. SCE, [13, 45, 46]), due to a mixed potential, arising from OH$^-$ ions interference [1]. The level of OH$^-$ ions interference will, therefore, depend on the chloride ions concentration (i.e., the OH$^-$/Cl$^-$ ratio) and will dominate in the absence of Cl$^-$ ions. A detection limit, largely determining a chloride sensor's response, is reported to be 10 mM chloride content [45]. Although OH$^-$ ions interference cannot be excluded in the hereby employed alkaline solutions of pH ca. 12.8, the chloride content in the model media was adjusted to be above the reported detection limit of 10 mM. This was also done in view of the objective of this work to elucidate the effect of AgCl morphology and microstructure on the response of sensor within chloride ions detection, rather than a silver oxide contribution to the sensors' performance.

OCP records

As already introduced, the sensors' response is the OCP record itself, reflecting the dynamic equilibrium at the sensor/environment interface. The main objective here was to determine the accuracy of the chloride sensors to reflect the chloride content in the alkaline medium. What should also be noted, is that the time to reach a stable OCP for each sensor will determine its sensitivity and stability. Since the model medium was identical, fluctuations or

unexpected performance would be related to the Ag/AgCl interface and/or the AgCl properties, respectively.

The OCP records in chloride-containing CE (20 and 260 mM chloride content) are presented in Fig. 4. As can be observed, increasing the chloride content from 20 (Fig. 4a) to 260 mM (Fig. 4b) results in a cathodic shift of the OCP values for all sensors. For sensors A and B, the initial values, e.g., within 60–120 s of immersion, read between 90 mV (for 20 mM chloride content) and 25 mV (for 260 mM chloride content), while before stabilization the initial OCP values for sensors C and D are between 40 (Fig. 4a) and 15 mV (Fig. 4b). At the end of the test, the final OCPs for all sensors correspond to the chloride content in the medium—for 20 mM chloride content, the adopted values were between 80 and 89 mV, for 260 mM solution—the final values were between 24 and 25 mV. This is as expected and reflects the relevant chloride content, since theoretically (following Eqs. 2 and 3), at 20 and 260 mM chloride concentration, a chloride sensor should read 89 and 23 mV versus SCE, respectively [45].

To be noted is that the OCP records in CE with 20 mM chloride concentration showed a variation of 50 mV at the beginning of the test, narrowing down to 7 mV after 7200 s (Fig. 4a). In 260 mM chloride-containing medium a smaller deviation was observed, i.e., less than 10 mV at the beginning of the test, decreasing to 1 mV after 7200 s (Fig. 4b). The results show that both OCP variation and the time needed for OCP stabilization are reduced upon an increase in chloride concentration from 20 to 260 mM. This is irrespective of the sensor type and anodization regime, respectively.

The results depicted in Fig. 4 also reflect a different pattern of performance for the different sensors: OCP stabilization depends not only on the chloride content in the medium, but also on the obviously different properties of the AgCl layer (which is in addition to the thickness variation, Fig. 3). As shown in Fig. 4a, approximately 60 s were needed for a stable OCP of sensors A and B, prepared at low current densities (Fig. 3), while more than 1800 s were required for sensors C and D (with a thicker AgCl layer, Fig. 3) to reach a stable value. This observation was relevant for both 20 and 260 mM chloride concentrations (Fig. 4a, b). The increase in the AgCl layer thickness from ~ 8 μm (sensor A) to ~ 15 μm (sensor B) has a negligible effect on the OCP stabilization time. However, the increase in AgCl layer thickness from 15 μm for sensor B to 20 μm for sensor C and 40 μm for sensor D, has an obvious influence on the OCP stabilization time. Consequently, the observed difference (1 min for sensors A and B vs. 30 min for sensors C and D) should be attributable to a specific AgCl layer morphology and microstructure, rather than to thickness alone. To be noted is that the above potential differences and deviation from the expected performance was also recorded in the same range for replicate specimens (three replicate specimens were tested, but results for these are not included in Fig. 4 for simplicity). For instance, in less than a 100 s, sensor A reached to the stable potentials of 85 ± 1.5
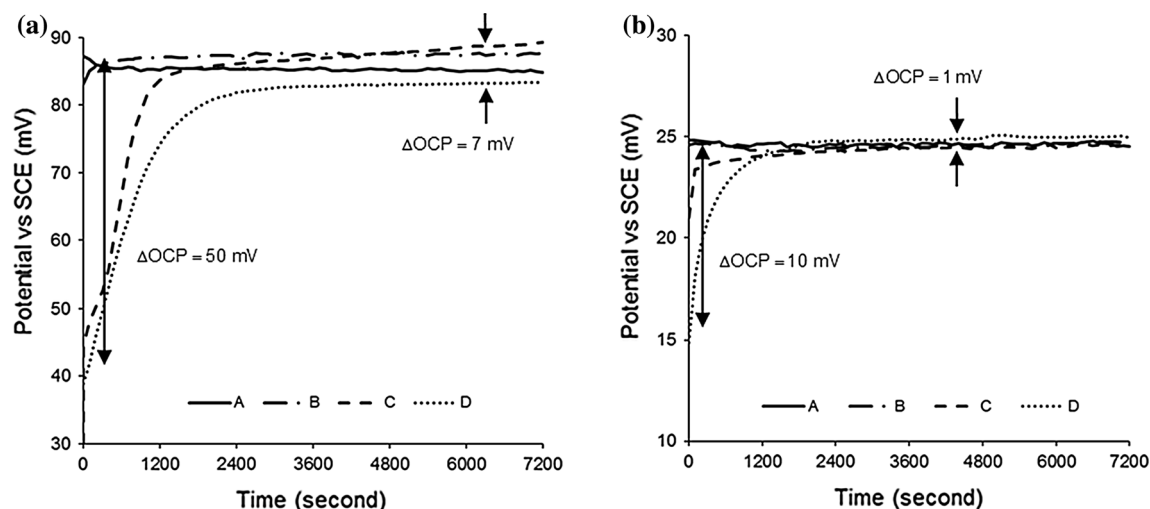
Fig. 4 Evolution of OCP values of the Ag/AgCl sensors in chloride-containing cement extract: **a** CE + 20 mM chloride content; **b** CE + 260 mM chloride content.

and 25 ± 0.2 mV in CE with 20 and 260 mM chloride concentrations, respectively. In contrast, a relatively stable OCP for the sensor D was observed after 1800 s, reading ca. 78 ± 3 mV for CE with 20 mM chloride concentration and 23 ± 2 mV for CE with 260 mM chloride concentration.

Additionally, the following observation is important to be specifically addressed: in the initial period, the higher instability of sensors C and D, compared to sensors A and B, was obvious (Fig. 4a, b, records prior to 1200 s). The result means that sensors C and D initially report an "overestimated" chloride content (a more cathodic OCP), while sensors A and B give an almost immediate accurate response. In other words, the potentially different microstructural properties of the Ag/AgCl interface for A and B versus C and D sensors should be responsible for the observed discrepancies. Except the already discussed considerations, this hypothesis follows the common knowledge that limitation of ion transport of any kind at the interface sensor/medium (or limitation of electron transport along the sensors' conductive surface) will be reflected in variations in the time to establish an equilibrium condition. These aspects will be discussed in "Correlation of sensors' response, surface properties and ohmic resistance of AgCl" section in correlation to the experimental results on microstructure of the Ag/AgCl interface. Surface chemistry, although supposed to be similar, might also play a role in the sensor's response. Therefore, the next step in this work is an in-depth investigation of the surface morphology, microstructure and surface chemistry of all sensors, which are discussed in the following sections.

## Surface morphology and microstructure

In this section, electron microscopy (Figs. 5, 6 and 7) and EDS analysis (Fig. 6) are discussed for all sensors (A, B, C and D), produced for identical anodization time of 1 h, but at different current densities (Fig. 3). Additionally, electron microscopy of the Ag/AgCl interface for D-type sensors, anodized at the highest current density of 4 mA/cm^2 and varying anodization time, is also presented (Fig. 7) as supportive evidence for the discussion in this and the next sections.

Figure 5 depicts ESEM micrographs from the top surface of the sensors, visualizing the AgCl layers, obtained in each anodization regime. As can be observed, the morphological features and packing of the AgCl layer are different in each case. For sensors A and B (Fig. 5a, b), "packed-piled" AgCl particles were well observed on the Ag substrate. Additionally, the AgCl layer appears to be relatively uniform, presenting rounded, 1–2 μm in (top) size AgCl particles, and a distinct boundary between these. Along with clearly observable boundaries, specifically for sensor A (Fig. 5a), well defined are the surface openings of micro-channels. For sensor B (Fig. 5b), these features become slightly distorted, the surface morphology, however, maintaining similar to the sensor A appearance.

In contrast, the AgCl layer for sensors C and D became a mosaic of complex patterns (Fig. 5c, d). The high current densities, as employed for 1 h in the production of sensors C and D (2 and 4 mA/cm^2), apparently induced the formation of elongated and discontinuous, "twisted" AgCl particles. The "inner" microstructure of the AgCl layer cannot be judged from surface observations only, but can be clearly visualized on a cross section of the Ag/AgCl interface. Figure 6 presents the cross sections for sensors A and D, together with relevant EDS analysis in depth of the sections, toward the Ag substrate (the results for sensors A and B were similar, as well as for sensors C and D, micrographs of the cross section for B and C sensors are, therefore, not presented). The EDS analysis in Fig. 6 for the interfaces in sensors A and D confirms both Ag and Cl in the AgCl layer, while only Ag at the Ag substrate, hence confirming the expected qualitative outcome for the Ag/AgCl interface.

For sensor A (Fig. 6a), a visually well adhered and homogeneous AgCl layer can be observed. The grain boundaries in depth of the layer can be well seen, showing a well packed and almost perpendicular orientation toward the Ag substrate. This upright particles' orientation would account for a continuous micro-channel network in depth of the layer. The contribution of such a morphology and microstructure to the performance of the sensor would be reflected in a rapid response to the environment. This is because a (vertically) open, continuous network of micro-channels would account for reduced limitations to ion transport. This was as actually observed, OCP records" section and Fig. 4, where an almost instant accurate response of sensors A and B to the pre-defined chloride content was recorded, together with a fast OCP stabilization. These microstructural
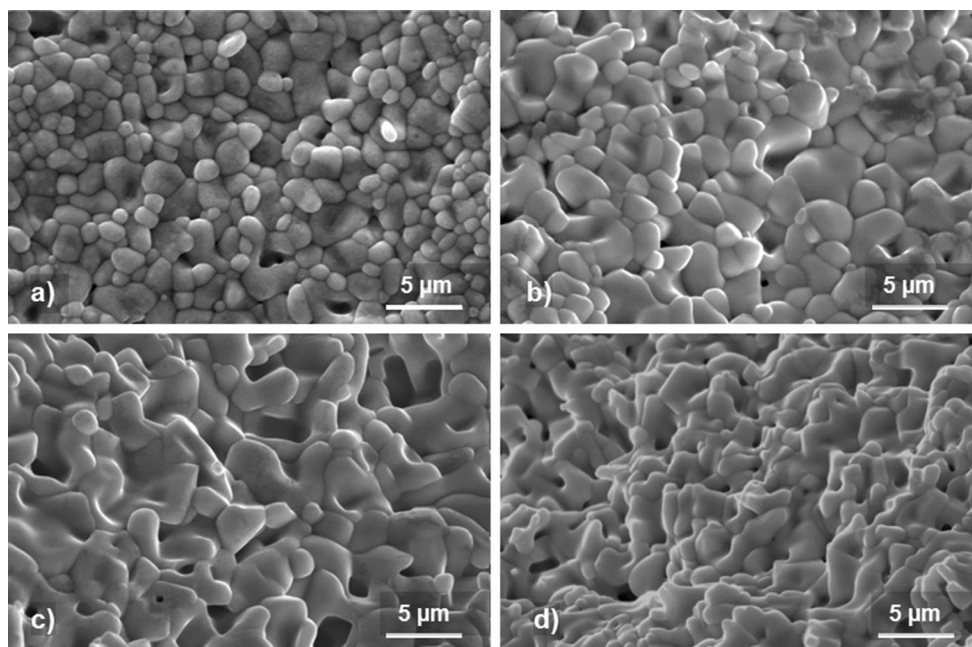
Fig. 5 ESEM images of the AgCl layer on the surface of sensors A at 0.5 mA/cm^2 (**a**), B at 1 mA/cm^2 (**b**), C at 2 mA/cm^2 (**c**) and D at 4 mA/cm^2 (**d**).
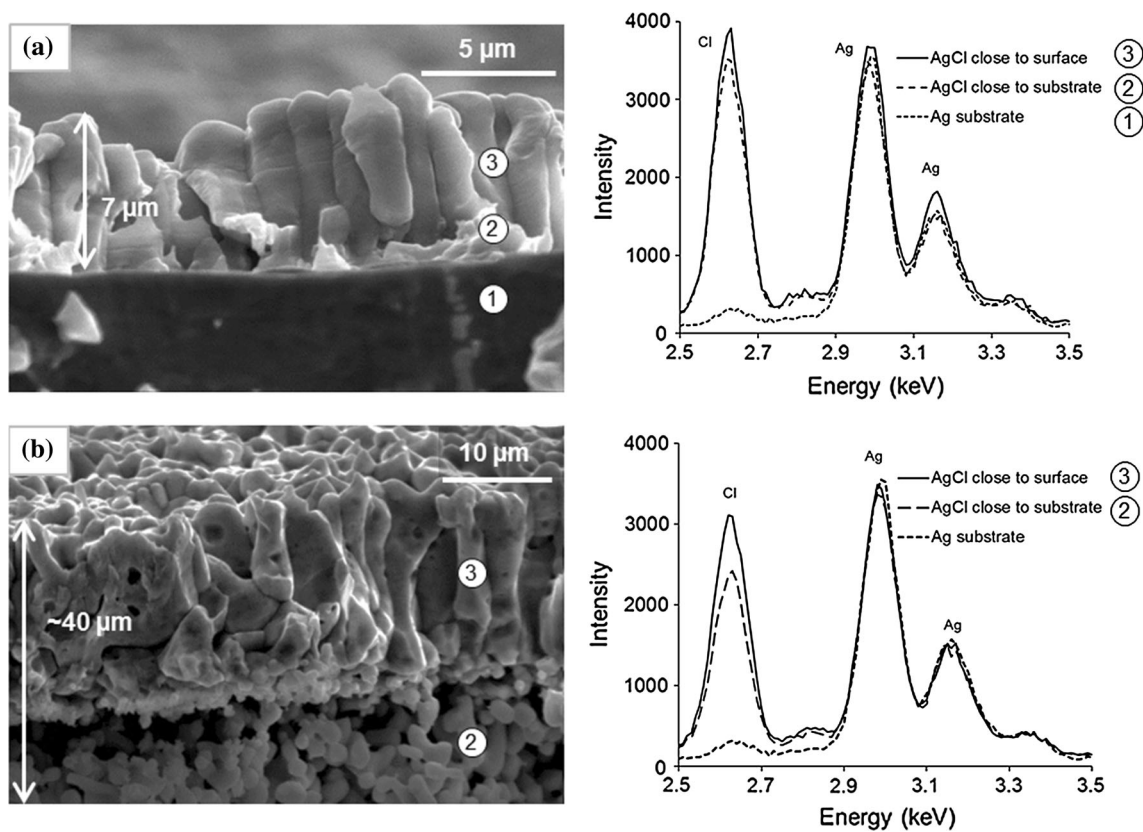
Fig. 6 Cross section and EDS spectra of the Ag/AgCl interface in sensor A at 0.5 mA/cm^2 (**a**) and sensor D at 4 mA/cm^2 (**b**). *Note* Ag substrate in (**b**) is not seen at this × 2500 magnification, which is chosen to allow visibility of the bi-layer structure in sensor D, together with the full AgCl layer thickness.
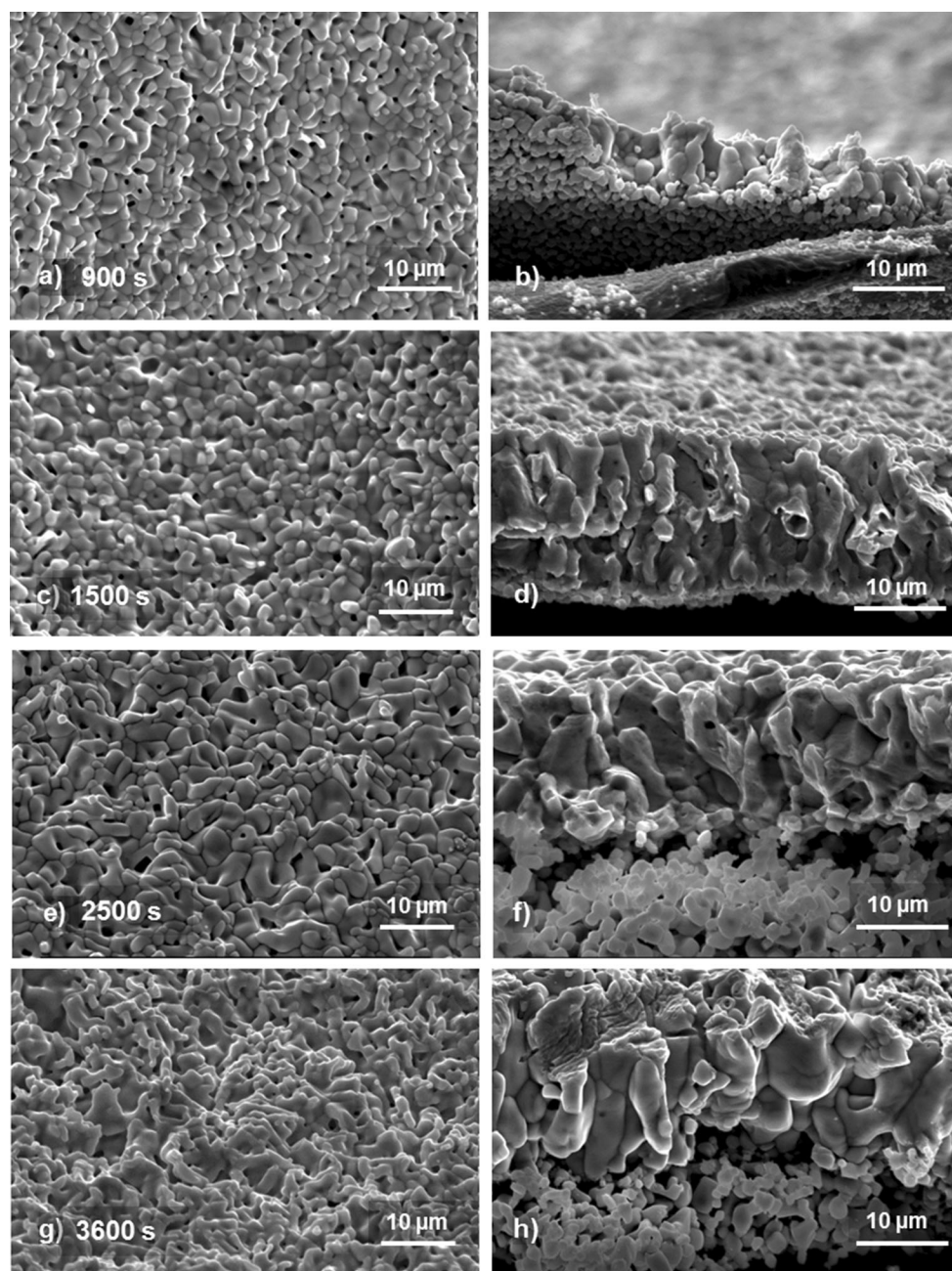
Fig. 7 ESEM images of the surface AgCl layer and cross sections of the Ag/AgCl interface for a D-type sensor, produced at 4 mA/cm^2 and varying anodization time: **a**, **b** 900 s, **c**, **d** 1500 s, **e**, **f** 2500 s, **h**, **f** 3600 s.

features versus the sensor' response will be discussed in "Correlation of sensors' response, surface properties and ohmic resistance of AgCl" section in more detail with regard to the ohmic (incl. ionic) resistance of the AgCl layer.

As shown in Fig. 6, increasing the current density from 0.5 mA/cm^2 (sensor A, Fig. 6a) to 4 mA/cm^2 (sensor D, Fig. 6b), indeed results in a thicker AgCl layer. The experimentally determined AgCl thickness

for each sensor was well in line with the theoretically approximated values (Fig. 3, "Sensors' response: OCP records" section). The higher current density, however, did not only result in the expected thickness increase, but also resulted in the formation of an additional inner layer of smaller AgCl grains, appearing close to the Ag substrate (Fig. 6b). For sensor D, Fig. 6b, a bi-layer appearance is obvious with an increased level of heterogeneity, visually not

as uniform and well adhered to the Ag substrate, as in sensor A (Fig. 6a). What can be also observed are a large number of occluded pores in the top (surface) portion of the AgCl layer (Fig. 6b). This feature, together with the "twisted" morphology of the ca. 20 μm top (surface) layer, would account for potentially increased ohmic, and ionic, respectively, resistance of the total (40 μm) AgCl layer overall, together with potentially increased tortuosity of the microchannel network. Along with the bi-layer structure, all these features would rise the limitations to ion transport and will be reflected in the response of sensor D, e.g., a delay in achieving a stable OCP would be relevant, as actually observed in Fig. 4.

Next to the above, the appearance of the Ag/AgCl interface in sensor D resembles features, previously reported in morphological studies of the Ag/AgCl interface after reduction cycles [11]. This accounts for the possibility of altered AgCl layer formation and reduction on the surface of the D sensors, resulting from the high current density during anodization. More importantly, the appearance of an inner layer of small AgCl grains, with open inter-grain pore spaces, can be an indication of weak adhesion of the top AgCl layer (or the AgCl layer overall) to the Ag substrate. This is especially considering the fact that the layer of smaller (AgCl) grains accounts for ca. 50% of the total thickness of AgCl on the D sensor's surface (Fig. 6b).

Summarizing, the microscopy studies revealed that Ag anodization for 1 h at the highest current density regime (sensors D) causes a high level of complexity, variation in morphological features and a distinct bi-layer structure of AgCl on the Ag substrate. Interpretation of these results can follow a hypothesis for a different AgCl formation mechanism on the Ag substrate at high current densities. These will be discussed in "Overall considerations" section in more detail with respect to the ohmic resistance of AgCl and the actual charge during anodization.

In order to support the above discussion and to present a stronger evidence for the effect of current density on morphology and microstructure of the resulting Ag/AgCl interface, Fig. 7 depicts ESEM micrographs of a sensor from type D, where anodization was performed at 4 mA/cm² only, but for varying time of anodization. The microstructural analysis of this D-type sensor was performed after 900, 1500, 2500 and 3600 s of Ag anodization. The last time interval (i.e., 3600 s) corresponds to the time of

1 h anodization, as previously discussed for all sensors A to D. Therefore, the features observed in Fig. 7g, f are similar to those in Figs. 5d, 6c for the previously discussed D sensor.

After only 900 s of anodization (Fig. 7a, b), the top surface of the AgCl layer already demonstrated the previously observed (Fig. 5c, d) AgCl particles with irregular shapes and a complex pattern (Fig. 7a). There was no clear evidence of a bi-layer structure after 900 s, although small grains appear to be present at the bottom portion of the AgCl layer (Fig. 7b).

The thickness of the AgCl layer after 900 s was 10 μm (Table 2 further below summarizes relevant information for this D-type sensor). With further increase in the anodization time to 1500 s, a thicker AgCl layer (15 μm) formed. At this stage, a bi-layer initiates to form with the contribution of small AgCl grains at the Ag substrate (Fig. 7c, d and Table 2). The small AgCl grains can also be found randomly in the bulk top layer (Fig. 7c, d). After anodization for 2500 and 3600 s, the morphology of the top surface of the AgCl layer was highly twisted and irregularly shaped (Fig. 7e, f). These were similar to the previously observed features in Fig. 6b, but here clearly pronounced for a shorter anodization time, i.e., after 2500 s. The cross section of the AgCl layer in these D-type sensors also revealed the presence of small AgCl grains and a bi-layer structure, with open inter-grain pore space (porous microstructure) near the Ag substrate (Fig. 7f, h). From the obtained results, it can be concluded that, the complexity and heterogeneity of the layer are irrespective of the anodization time. However, the appearance of a bi-layer structure in D-type sensors is anodizing time dependent. The formation of small AgCl grains was also well observed, together with interlayer cavities and irregular empty space. All these features appear in less than 1 h and, as previously discussed, would increase the potential of de-bond or reduced adhesion of the AgCl layer on the Ag substrate, subsequently would affect the sensors' performance.

Following the results and discussion in this section, the surface morphology and in-depth microstructure of the AgCl layers in sensors A–D are obviously different and current density dependent. Such differences would logically lead to a variation in electrochemical response, when the sensors are in contact with the external environment. This was as actually observed (Fig. 4) and discussed with respect to the OCP records in "Sensors' response: OCP records"

section. The highest instability in the model medium was recorded for sensors D, while an almost immediate stable state was achieved for sensor A.

From the abovementioned, the AgCl layer thickness, morphology and microstructure for sensors A–D are significantly different. It was hypothesized that these variations would be responsible for potentially different surface chemistry, although AgCl will be predominant (as detected by qualitative EDX analysis). For a more in-depth and quantitative analysis of the surface chemistry of sensors A to D, XPS analysis was performed, results and discussion on which are presented in the next section.

Surface chemistry and composition

The high-resolution XPS spectra for all sensors are presented in Fig. 8. Figure 8a depicts the Ag3d spectra. The characteristic 3D states of different Ag compounds and metallic Ag (Ag^0) are very close to each other, i.e., within 0.5 eV [47, 48]. Hence, the binding energy positions of Ag3d do not unambiguously identify the actual state of Ag. To support the derived information from binding energy records, the AgMNN Auger peaks were used (Fig. 8b). For comparative purposes, the AgMNN peak for Ag^0 is

shown in Fig. 8b. The Auger parameter ($\acute{a} = EK(AgMNN) + EB(Ag3d^{5/2})$) was used for a more accurate determination of the chemical state of Ag, thus eliminating the surface effects of electrostatic charging [49]. The binding energy for oxygen (O1s) is also presented in Fig. 8c. The obtained surface atomic concentrations are given in Table 1. The XPS analysis does not claim absolute values for chemical composition of the AgCl layers, but provides an accurate (quantitative) comparison of equally handled samples for the purposes of this work.

Before a detailed analysis of the XPS results in Fig. 8, the following should be noted. The process of Ag anodization in 0.1 M HCl (pH 1.4) results in electro-formation of a AgCl layer on the Ag substrate. As discussed with relevance to the electrochemical tests of Ag in 0.1 M HCl solution, also supported by the CV test results (Fig. 2, "AgCl nucleation and growth" section), 0.1 M HCl as a medium for sensors' preparation prevents Ag_2O formation, and favors AgCl formation. Consequently, any other compounds, as detected by XPS, were considered as impurities on the sensors' surface. The amount of impurities, however, and/or recombination of these, can be a consequence of the current density regime
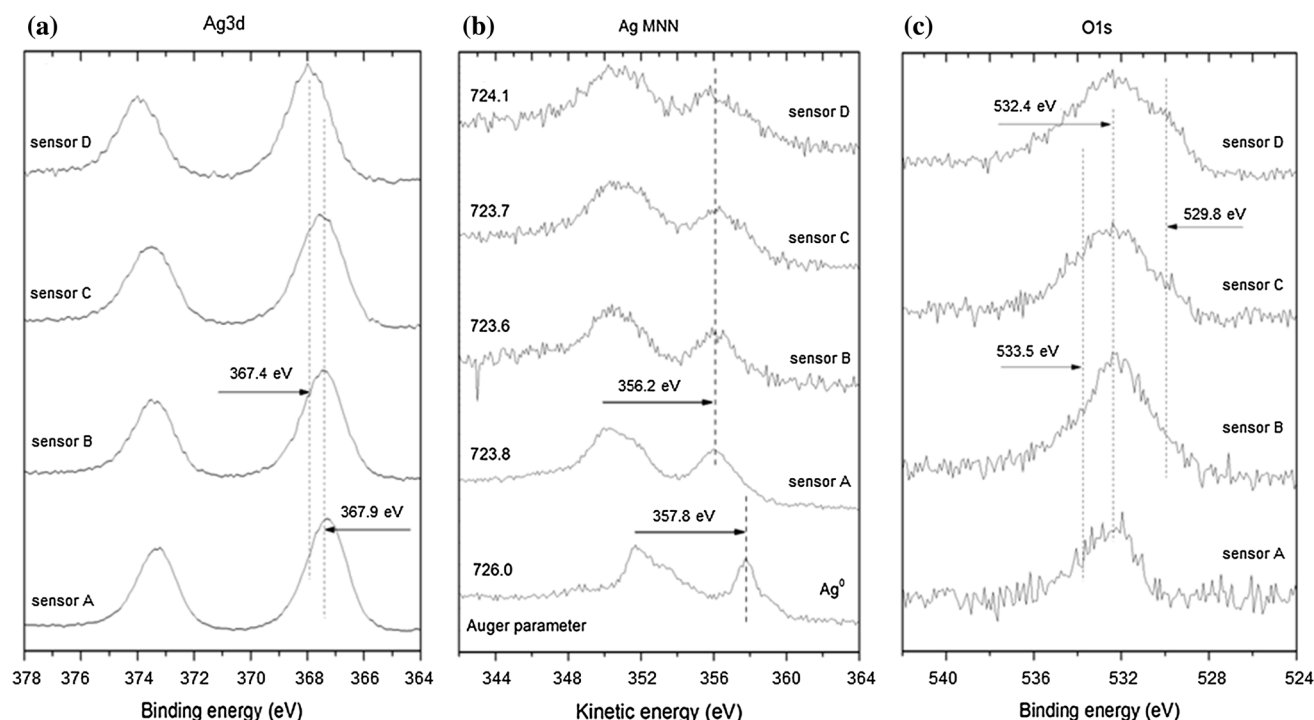
Fig. 8 High-resolution XPS spectra for all sensors after 1 h anodization (A at 0.5 mA/cm^2, B at 1 mA/cm^2, C at 2 mA/cm^2 and D at 4 mA/cm^2): **a** Ag3d photoelectron lines; **b** AgMNN—Auger lines and **c** O1s photoelectron lines.

Table 1 Surface atomic concentration (at. %) of the AgCl layer for all studied conditions (carbon (C1s), silver (Ag3d), chloride (Cl2p), Oxygen (O1s))

Anodization regime	C1s (%)		Ag3d (%)	Cl2p (%)	O1s (%)
	C–C; C–H	C–O			
A	19	12	27	34	8
B	41	28	8	13	10
C	42	25	10	13	10
D	59	19	3	5	14

and different thickness, morphology and adhesion of the AgCl layer on the Ag substrate. Hence, the XPS surface analysis provides a strong supportive information for the performance of all sensors. The XPS results also elucidate the dependence of the sensors' electrochemical response on surface morphology and microstructure.

XPS analysis for sensors A and B

The Ag3d$^{5/2}$ core level for sensor A was measured at 367.4 eV (Fig. 8a), which is attributed to Ag$^+$ in AgO [47]. The kinetic energy of the AgMNN peak for the same specimen was measured at 356.2 eV (Fig. 8b), which slightly differs (0.5 eV) from the corresponding energy for AgO. The binding energy of the O1s peak for the same sensor A (Fig. 8c) was measured at 532.4 eV, attributed to Ag–C–H–O and/or OH$^-$. Hence, the O1s binding energy strongly differs from 530.7 eV for O1s in AgO. Additionally, the Auger parameter exhibits a value of 723.8 for sensor A. This value falls in the range between 723.5 (for AgCl) and 724.2 (for AgO). The recorded atomic concentrations ratio for sensor A (Table 1) for Ag:Cl:O equals 3.4:4.2:1. Consequently, the presence of AgO on the surface of sensor A is not justified.

For sensor B, similar binding energies as those for sensor A were recorded, although, as would be expected for a thicker AgCl layer (as in sensor B), a slightly broader AgMNN peak was observed, if compared to that in sensor A (Fig. 8b). The Auger parameter for sensor B with a value of 723.6 is closer to that for AgCl (723.5) [47]. The surface atomic concentration for sensor B (Table 1) gives a ratio between Ag:Cl:O = 0.8:1.3:1.

It can be concluded that the surface composition of sensors A and B is similar, also in line with the recorded similar surface morphology and microstructure ("Surface morphology and microstructure" section). These explain the close OCP

response of sensors A and B to a pre-defined chloride content ("Sensors' response: OCP records" section).

XPS analysis for sensors C and D

The photoelectron lines and the Auger peaks for sensors C and D are already different from these for sensors A and B. Broadening of the Ag3d peak and a shift of the binding energy toward higher values were observed (Fig. 8a). The binding energy of 367.5 and 367.9 eV was measured for sensors C and D, respectively. The broadening of the Ag3d peak is related to the presence of subpeaks, characteristic for silver in a different state. This is also evident from the AgMNN peaks (Fig. 8b), where the kinetic energies of 356.2 and 357.8 eV were measured, corresponding to Ag^{2+} and Ag^0, respectively. The shape of the AgMNN peak line is similar to the shape measured by Ferraria et al. [48] for a mixed silver–silver oxide electrode. Additionally, several binding energies were obtained from the O1s peaks for sensors C and D (Fig. 8c). The O1s binding energy with the highest intensity at 532.4 eV corresponds to Ag–C–H–O, whereas the significantly more pronounced peak with a binding energy of ca. 530.0 eV is ascribed to Ag$_2$O and/or AgO. The wide shoulder of the O1s peak at 533.5 eV corresponds to OH$^-$ and to adsorbed water. The concentration ratio between elements, present on the surface is Ag:Cl:O = 1:1.3:1 for sensor C, and Ag:Cl:O = 4.67:2.8:1 for sensor D.

As above concluded for sensors A and B, the XPS results for sensors C and D are strongly supportive the microstructural observations. Additionally, the different surface chemistry, as recorded through XPS for sensors C and D, explains the distinctly different electrochemical response to alkaline medium with pre-defined chloride content ("Surface chemistry and composition" section).

Correlation of results on surface analysis

Considering the above XPS results, it can be stated that the surface of all sensors is mainly AgCl covered, with the presence of impurities as AgO, Ag_2O and Ag–C–H–O. The concentration of silver oxide and Ag–C–H–O increases with the increase in applied anodization current density. The "purity" of surface AgCl is in the order of: A > B ∼ C > D. Therefore, among all sensors, sensor A contains purely silver chloride at the most. The impurities increase in sensors B and C, while the highest level of impurities was observed in sensor D, where a more significant amount of compounds, different from AgCl were present. These results (together with the different morphology and microstructure, "Surface morphology and microstructure" section) explain the variation in establishing a stable state for the different sensors in alkaline medium ("Surface chemistry and composition" section).

The significant difference in atomic concentrations for Ag3d and Cl2p between, e.g., sensors A and D (Table 1) is most likely linked to additional chemical recombination in depth of a thicker and more heterogeneous bi-layer of AgCl (as in sensors C and D), rather than surface adsorption and contamination only. This is because, on the one hand, simply blocking the surface by impurities from the environment would be detected as adventitious hydrocarbons and CO of increasing concentration during the XPS investigation, which was not the case. On the other hand, for specimen D, the surface layer is not AgCl only, but a composite structure, with a significant contribution of metallic Ag, AgO and C-based compounds. The presence of metallic Ag is well evident—Fig. 8a, Ag3d at 367.9 eV—denoted to Ag^0, together with a well pronounced broadening, a shoulder at 357.8 eV for Ag^0 in the AgMNN Auger line for sensor D (Fig. 8b). Additionally, the broad O1s peak with a shoulder at 529.8 eV, as visible in the O1s photoelectron line (Fig. 8c), account for the largest contribution of AgO in the case of D, compared to all other cases. The presence of C-based compounds is most likely related to a large extent to the (electro) chemical transformations within the process of anodization (lab air), in the sense that: enhanced surface area of the D sensor, together with the well-known catalytic activity of Ag toward CO_2 reduction reactions, will bring about not only C-based

compounds formation, but also reduction of Ag^+ to metallic silver [50].

To this end, a synergetic effect of the increasing thickness, roughness and bi-layer structure of the AgCl for the case of sensor D (as in fact observed and discussed in the previous sections), would account for a more pronounced chemical recombination and transformation of the AgCl layer if compared to the case of, e.g., sensors A.

As above shown in "Surface morphology and microstructure" section and 3.4, the AgCl layer morphology, microstructure and chemical composition vary and depend on the applied current densities within the anodization regimes. Higher current densities result in thicker AgCl layers (as expected), increased complexity (e.g., more than one interface was observed) as well as higher impurities and chemical recombination within the layer. These subsequently influence the potentiometric response of the sensors in alkaline environment and ultimately result in variations of sensors' stability, as recorded and discussed in "Sensors' response: OCP records" section.

## Correlation of sensors' response, surface properties and ohmic resistance of AgCl

Overall considerations

As discussed in the previous sections, the process of Ag anodization involved the application of a constant current at a chosen current density level. In the medium of 0.1 M HCl, this results in the formation of a AgCl layer of a certain thickness, morphology and compactness. Figure 9 schematically presents a AgCl layer, formed on the surface of a Ag wire, as used in this study. The boundaries between the AgCl particles and the pore channels through the layer, known as micro-channels, are also indicated (Fig. 9a–c). These micro-channels are the main pathways for the transport of ions within the AgCl layer [51, 52] and develop differently with respect to the anodization regime (Fig. 9b, c). As the AgCl layer thickens, ion transport becomes limited due to micro-channels confinement. This will be reflected by changes in the electrochemical response of the Ag/AgCl interface during anodization, and will be recorded as overpotential changes. In other words, while the applied current is maintained constant, the potential will reflect the above limitations and the electrochemical
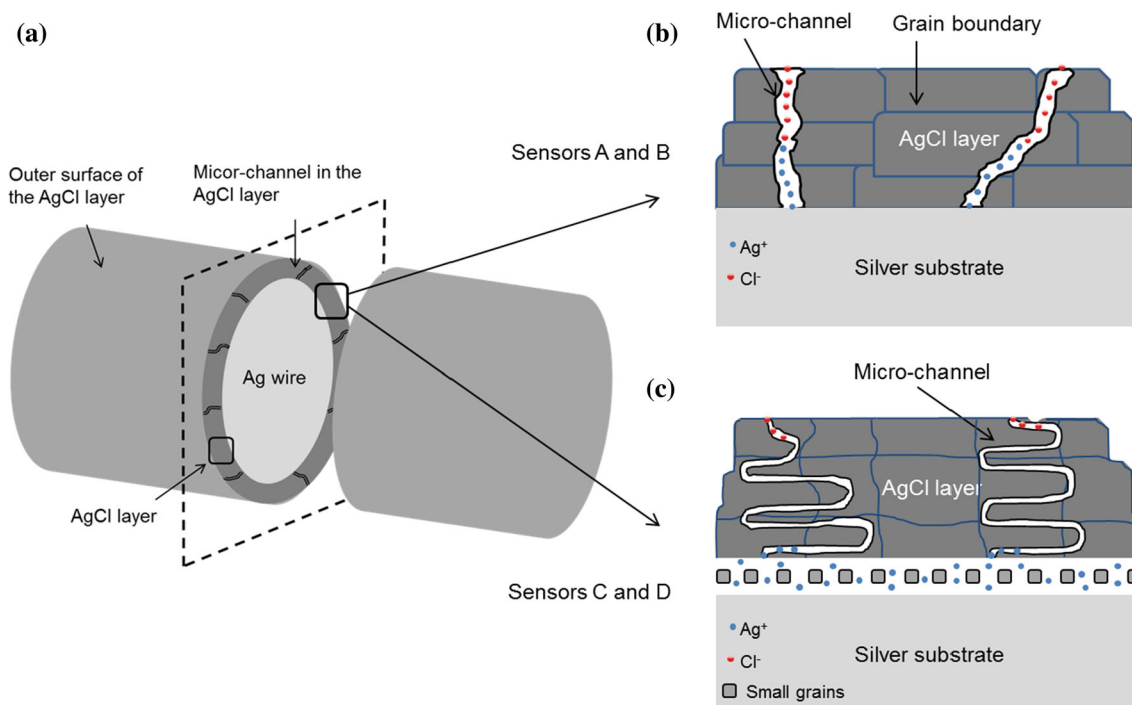
Fig. 9 Schematic of a Ag/AgCl sensor: **a** AgCl layer on the surface of a Ag wire; **b** AgCl layer as produced at lower current density regimes of 0.5 and 1 mA/cm^2 (sensors A and B); and **c** AgCl layer as produced at higher current density regimes of 2 and 4 mA/cm^2 (sensors C and D).
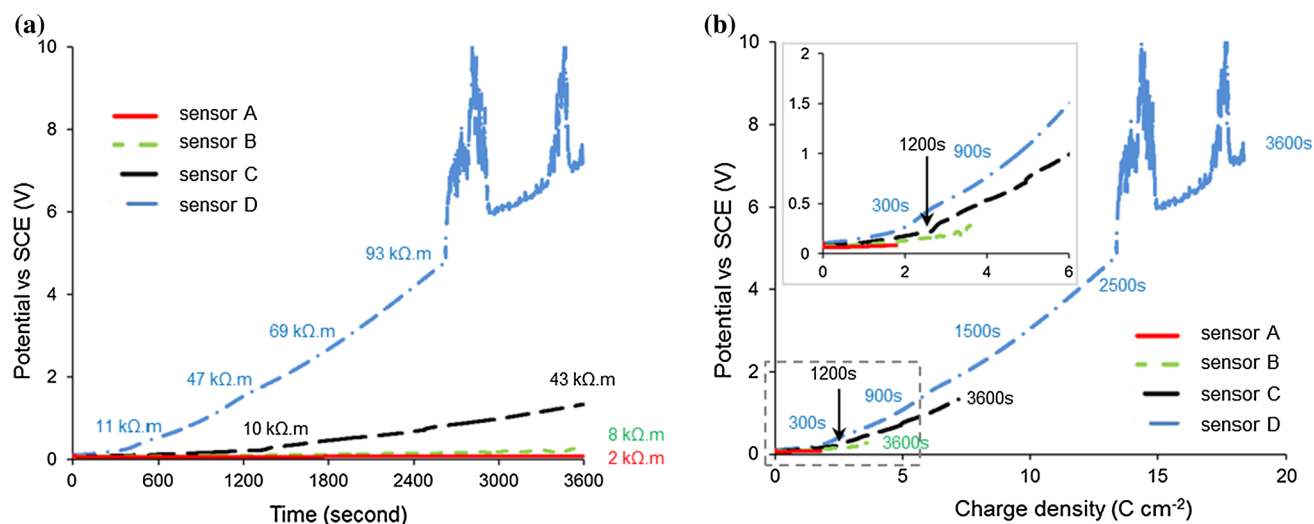
Fig. 10 Overpotential vs time (**a**) and overpotential vs charge density (**b**) during anodic formation of AgCl on a Ag wire in 0.1 M HCl in regimes A (0.5 mA/cm^2), B (1 mA/cm^2), C (2 mA/cm^2) and D (4 mA/cm^2).

interface will respond by an increase in overpotential. Figure 10a depicts the experimentally derived overpotential increase during 1 h anodization in the previously discussed (Fig. 3) regimes A, B, C and D, i.e., during the production of sensors A–D, respectively.

Figure 10 also presents the relation of overpotential increase versus the actual charge density during anodization for all sensors. Both potential versus time (Fig. 10a) and potential versus charge (Fig. 10b) curves provide information, linked to the physical properties of the AgCl layer during anodization and

are related to the layers' formation, possible restructuring, surface roughness and/or limitations to further growth.

The inflection points in the curves reveal the point(s) of AgCl layer alterations during anodization. Consequently, a linear relationship as in regimes A and B (Fig. 10) accounts for a uniform and continuous AgCl formation—as in fact observed for sensors A and B. The overpotential response is well in line with the actual morphological, microstructural and surface chemistry results for the low current density regimes A and B ("Surface morphology and microstructure" section and 3.4).

A semi-linear relationship, as in regime C (nonlinearity between 900 and 1200 s, Fig. 10a, b), already accounts for events of restructuring and increased heterogeneity of the layer. This is also in line with the surface analysis for sensor C, resembling features and surface chemistry close to sensor D. The most significant nonlinear response in Fig. 10 was for regime D—here thickening and restructuring of the AgCl layer are expected to be at the highest level. These were also as observed, presenting a bi-layer structure on the surface of sensor D, together with the presence of small AgCl grains and inter-grain voids and cavities (Figs. 5d, 6b and 7).

Overpotentials in high current densities regimes—sensors D

As shown in Fig. 10a, b, the nonlinear response of sensor D can be segmented as follows: an increase in overpotential was recorded starting after ca. 300 s, significantly more pronounced after 900 s (Fig. 10a, b); followed by further increase after 1500 s and an abrupt rise of overpotential after 2500 s, together with intensive fluctuations at the end of the test. At values above 4.5 V, the overpotential for regime D showed an abnormal fluctuation, related to passivation-like behavior or significant increase in surface roughness.

Such fluctuations (erratic polarization response), as in the 4 mA/cm^2 regime for sensor D, were reported to result in evolution of oxygen and chlorine on the surface of the substrate [6], which would (at the very least) cause surface heterogeneity and changes in surface chemistry. For sensors D, the former was reflected in a "twisted" AgCl layer morphology (Fig. 5d), and a bi-layer structure of the AgCl on the Ag surface (Figs. 6b and 7). The latter, changed

surface chemistry, is reflected in a more significant contribution of AgO and Ag–C–H–O-based compounds in the AgCl layer of sensors D, as derived by XPS analysis ("Correlation of results on surface analysis" section). In fact, well known is that high overpotential and oxygen evolution will be relevant during anodization at high current densities (as in the case of sensor D, Fig. 10). Depending on the pH of the medium, oxygen evolution occurs on a metal electrode, following one of the below reactions:

$$4OH^- \leftrightarrow 2H_2O + O_2 + 4e^- \tag{6}$$

or

$$2H_2O \leftrightarrow 4H^+ + O_2 + 4e^- \tag{7}$$
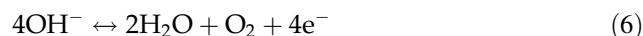
During anodization of the Ag wires in a low pH medium (0.1 M HCl of pH 1.4), the OH$^-$ concentration was limited; therefore, the oxygen evolution on the metal (Ag in this case) surface will be a result from the reaction in Eq. (7). The overpotential for oxygen evolution can be calculated by Eq. (8).

$$\eta_{O_2} = E_{O_2/OH^-} - E_i \tag{8}$$

where η_{O_2} is the overpotential of oxygen evolution, E_{O_2/OH^-} is the equilibrium potential of the oxygen electrode (determined by Eq. 9) and E_i is the potential of the metal under polarization (or the potential of Ag during anodization in this case).

$$E_{O_2/OH^-} = 1.299 - 0.059pH \tag{9}$$

Additionally, well known is the unstable character of the oxygen electrode in general, which is due to the irreversible character of the electrochemical reactions as given by Eqs. (6) and (7). Irreversibility (limitation of the reactions in Eqs. (6) and (7) from right to left) is a consequence of nonreversible surface modification of the metal electrode, as for instance due to oxidation of the metal surface or transformation of the oxygen gas phase to OH$_2^-$ ions. The result for the metal electrode is a nonstable and nonreproducible potential. This is in addition to the fact that, following Eq. (9), an anodic oxygen evolution in low pH medium can only occur at potentials significantly more positive than 1.299 V. Additionally, at significantly positive potentials the metal surface will be electrochemically altered, e.g., enhanced dissolution of the substrate or passivation will be relevant. In both cases a substantial surface modification of the original metal substrate will be at hand.

The above considerations and electrochemical aspects/phenomena are directly applicable to the sensor D, where clearly, surface modification during the anodization process was relevant if overpotential evolution is taken into account (Fig. 10a, b). Microstructural studies ("Surface morphology and microstructure" section) and surface chemistry analysis ("Surface chemistry and composition" section) confirmed the electrochemically altered Ag/AgCl interface and explain the nonstable electrochemical state of sensor D in the model medium ("Sensors' response: OCP records" section).

Surface chemistry, microstructure and ohmic resistance of the AgCl layer

Except the above-discussed aspects in relation to overpotential and surface of the sensors, abnormal overpotential evolution would be attributable to an increase in thickness but also, in general, reflecting an increase in ohmic resistance of the surface layer [8]. The ohmic resistance, however, is a combination of both ionic and electron resistance. In the case of a Ag/AgCl interface, where the AgCl layer contains nonconductive solid AgCl particles, the effective conductivity of the surface (AgCl) layer overall depends on the presence of micro-channels (as schematically shown in Fig. 9b, c) and the resulting ionic conductivity. In other words, the ionic resistance (and ionic conductance, respectively) of the AgCl layer will be a dominating factor for ion transport, surface changes, and ultimately—sensor's response in the model medium.

The ionic resistance (resistivity, respectively) of the AgCl layer during anodization can be analytically derived by employing the results in Fig. 10 and Eq. (10). The linear increase in overpotential (ΔE) with charge density (ΔQ) is presented as follows, [11]:

$$\frac{\Delta E}{\Delta Q} = \rho J V_0 / F \tag{10}$$

where "ρ" is the ionic resistivity, "J" is the current density, "V_0" is the molar volume of the AgCl (25.8 cm^3 mol^{-1}) and "F" is the Faraday constant (96485.3329 s A/mol).

To determine the ionic resistivity, a linear regression of the potential versus charge curves in Fig. 10b was performed with an accuracy for the A and B sensors of $R^2 > 0.99$, where R^2 is the coefficient of determination with linear regression. The coefficient

of determination (R^2) is the key output of regression analysis. It accounts for the deviation of the experimental data points from the values predicted by the linear regression equation. For sensors C and D, a nonlinear relation was recorded; therefore, the curves in Fig. 10b were segmented into linear portions. The resulting coefficient of determination was again $R^2 > 0.99$ for these linear portions. Table 2 summarizes the calculated values for thickness and ionic resistivity of the AgCl layer for each regime and sensor, respectively.

For sensors A and B, the layer thickness between 6 and 17 μm (theoretically calculated and experimentally derived, Fig. 3 and Table 2) corresponds to a relatively low ionic resistivity between 2 and 8 kΩ m. Low resistivity is well in line with the actual ESEM microstructural observations, where a compact and homogeneous, yet open micro-channel top surface was recorded for sensors A and B (Fig. 5a, b). Together with the low to insignificant amount of impurities as recorded by XPS analysis ("Surface chemistry and composition" section) the AgCl layer for sensors A and B would present the lowest (overall) ohmic resistance. This will yield higher ionic conductance of the AgCl layer and reduced limitations to ion transport (Fig. 9b). In turn, the above will account for a rapid stabilization of electrochemical equilibrium at the Ag/AgCl interface and fast OCP stabilization, as actually recorded ("Sensors' response: OCP records" section).

For sensor C, the AgCl layer thickness increased disproportionally to the already higher current density during anodization, i.e., 2 mA/cm^2 (Fig. 3, Table 2). Based on the two linear segments of overpotential versus charge response (Fig. 10b), the overall thickness of 20 μm corresponds to an ionic resistivity of maximum 43 kΩ m. This result is already an indication of the nonlinear relationship between layer thickness and ionic (ohmic) resistance, suggesting a dependence of the AgCl layer resistive properties on structure, morphology and composition. This hypothesis will be better illustrated if sensor D and the D-type sensors are discussed, which is in what follows.

Table 2 presents the measured thickness of the AgCl on the surface of sensor D (Figs. 6b and 7), together with the calculated ionic resistivity per linear segment of the response in Fig. 10b. As can be observed, increasing the thickness of the AgCl layer is not proportional to the increase in ionic resistivity.

Table 2 Ionic resistivity of the AgCl layer at different current densities and anodization time

Regime	Current density (mA/cm^2)	Measured thickness (μm)	Anodization time (s)	Charge density (C cm^{-2})	Ionic resistivity (kΩ m)
A	0.5	6–10	0–3600	< 1.8	2
B	1	12–17	0–3600	< 3.6	8
C	2		0–1200	< 2.4	10
		∼20	1200–3600	2.4–7.2	43
D	4		0–300	< 1.6	11
		∼10	300–900	1.6–4.8	47
		∼15	900–1500	4.8–8.6	69
		∼30	1500–2500	8.6–13	93
		∼40	2500–3600	N/A	N/A

For instance, if the rapid increase to ca. 70 kΩ m upon thickness increase to 15 μm (Table 2) is considered, a layer thickness of 30 μm (after 2500 s anodization) would be expected to present an ionic resistivity in the range of 140 kΩ m instead of the recorded 93 kΩ m. This nonproportionality is attributable to the: actual morphology and microstructure of the AgCl layer in sensors D; the potentially high tortuosity of the micro-channel network (Fig. 9c); the occluded pores and the gaps and voids in the bi-layer structure (Figs. 6b and 7). These features account for a limited ion transport, reflected by the increased ionic resistivity of the AgCl layer in sensor D.

The correlation of ionic resistivity and microstructure of the AgCl layer is discussed next in view of the aspects: intrinsic conductivity, extrinsic conductivity and conduction mechanisms of AgCl growth during anodization.

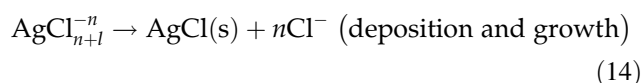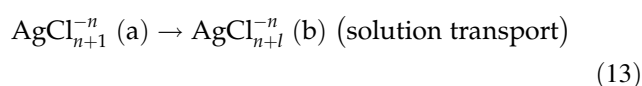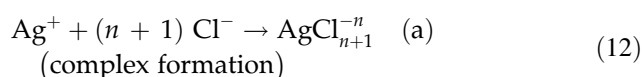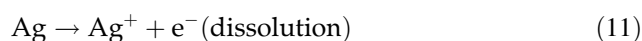*Intrinsic and extrinsic conductivity of the AgCl layer*

In conditions, when the transport of ions in the AgCl layer is limited (as in sensor D), schematically shown in Fig. 9c, due to concentration and/or resistance polarization, the rate of overpotential increase (Fig. 10) is controlled by two processes: (1) migration/diffusion of Ag$^+$ ions away from the Ag substrate into the bulk solution and, conversely, (2) chloride ions from the bulk solution toward the Ag substrate (Fig. 9c). The continuous formation of AgCl blocks the micro-channels, and decreases their radii with time. Eventually, the blockage and reduced number of micro-channels will increase the tortuosity and the transport distance of ions within the layer. At this stage, a sequence of incipient "crack" formation

and "healing" of the already available cracks occurs [8]. The cracks are actually a slight broadening of the micro-channels, already existing in the layer. In this case, the AgCl growth follows the so-called low-field conduction mechanism [12].

The decrease in the number of open micro-channels and the decrease in conductivity of the layer, may lead to a reversal of the conduction mechanism from micro-channel-controlled (extrinsic conductivity) to AgCl solid phase-controlled (intrinsic conductivity) [5]. This is known as high field conduction. AgCl is a poorly conducting solid (1.2×10^{-7} S/cm) with large concentrations of ionic defects (Ag$^+$) that range up to 0.7% of the lattice ions near the melting temperature [53]. The contribution of interstitial Ag$^+$ to the migration of ions through the AgCl solid results in intrinsic conductivity of the AgCl layer [54]. These mechanisms can explain the different morphology and microstructure of the AgCl layers, obtained at equally high current density (4 mA/cm^2) and varying anodizing time (D-type sensor in Fig. 7) or obtained at different current densities, but equal anodization time (1 h duration) (sensors A–D in Fig. 5 and 6).

Additionally, at high overpotential (e.g., sensors C and D, Fig. 10), the low ionic conductivity of the AgCl layer limits the transport of silver ions (Ag$^+$) away from the Ag substrate into the bulk solution (as schematically shown in Fig. 9c). At the same time, sufficient amount of chloride ions is available at the interface between the AgCl layer and the solution to react with the Ag$^+$, hence, forming the AgCl complexes, $[AgCl_n]_{(aq)}^{(1-n)}$ [55]. A part of $[AgCl_n]_{(aq)}^{(1-n)}$ would diffuse inward, encountering a region with

lower chloride content. These interactions favor the nucleation and growth of AgCl particles from the liquid phase in the bulk of the AgCl layer [56, 57]. The increased tortuosity of the outer surface of the AgCl layer is due to the ongoing formation of $\left[\text{AgCl}_n\right]_{(aq)}^{(1-n)}$ and possible absorption of impurities such as CO_2 [50]. The absorption of impurities at the surface of the AgCl layer was previously discussed in "Surface chemistry and composition" section. The XPS analysis provided a strong supportive evidence for the presence of carbon-based impurities and AgO at the surface of sensors C and D. The formation/dissolution of $\left[\text{AgCl}_n\right]_{(aq)}^{(1-n)}$ is in accordance with the following subsequent Eqs. (11)–(14):

$$\text{Ag} \rightarrow \text{Ag}^+ + \text{e}^- \text{ (dissolution)} \tag{11}$$

$$\text{Ag}^+ + (n+1)\,\text{Cl}^- \rightarrow \text{AgCl}_{n+1}^{-n} \quad (a) \atop (\text{complex formation}) \tag{12}$$

$$\text{AgCl}_{n+1}^{-n}\ (a) \rightarrow \text{AgCl}_{n+l}^{-n}\ (b)\ (\text{solution transport}) \tag{13}$$

$$\text{AgCl}_{n+l}^{-n} \rightarrow \text{AgCl}(s) + n\text{Cl}^- \text{ (deposition and growth)} \tag{14}$$

The development of intrinsic and diffusion-controlled conductivity of the AgCl in sensors C and D are the causes for a significant contribution of Ag^+ close to the silver substrate and dissolution/growth of the AgCl layer [58, 59]. These processes subsequently result in the appearance of small grains close to the silver substrate, but also embedded in the top AgCl layer (Figs. 6b and 7d, f, h). The reduced amount of chloride ions in this region most likely facilitates the formation of metallic silver (Ag^0) in the bi-layer structure of AgCl. This is also linked to the expected presence of Ag^0, due to substrate dissolution (as previously discussed in "Overpotentials in high current densities regimes: sensors D" section) at the recorded overpotentials of > 4 V, Fig. 10b. Although the EDS results indicate these small grains to be AgCl, the analysis is in fact masked by the surrounding AgCl matrix; hence, interpretation is not straightforward but only qualitative. Therefore, it is well possible that in fact the small grains are metallic Ag-based, deposited on the Ag substrate, as well as ingrained in the overall AgCl layer toward the surface of the sensors. The significant contribution of Ag^0 at the outer surface of sensors C and D, as defined by XPS analysis ("Surface chemistry and composition" section), confirms the above plausibility.

Considering the above discussion and the sensors' response to pre-defined chloride content (OCP records in Fig. 4, "Sensors' response: OCP records" section) the following can be summarized for the dependence of the sensors' stability on AgCl microstructure and surface chemistry. The packed AgCl particles at the surface of sensors A and B would determine a certain activity for silver ions (Ag^+) close to the silver substrate. In the presence of chloride ions penetrating from the external environment, the Ag^+ activity will change to establish a new equilibrium at the sensor's surface ($\text{Ag} + \text{Cl}^- \text{ - AgCl} + \text{e}^-$). A fast equilibrium is achieved in a short period of time, which reflects a stable OCP response of sensors A and B in the solution. In the presence of impurities, such as Ag^0 in sensors C and D, a lower concentration of Ag^+ will be available at the surface of the Ag substrate. The decreased concentration of Ag^+ would subsequently shift the sensor's OCP toward more negative (cathodic) potentials [59]. This is also in accordance with the Nernst equation and more negative potential of the Ag/Ag^+ electrode at lower silver ions activity. Therefore, a longer time is needed for the establishment of an equilibrium condition at the sensors' C and D surface. This time period depends on the chloride concentration in the medium and is shorter, when the chloride concentration is increased (Fig. 4b).

In view of the practical application of these sensors in alkaline medium, for instance cement-based materials, the following needs to be noted: the results and discussion in this paper refer to lab tests for short time periods and answer the objectives of this work. Although clearly sensors A perform best, their long-term performance, together with the long-term behavior of all other sensor types, is necessary to be considered next.

This paper does not include the long-term testing of the discussed sensors. However, the following points can be noted with regard to practical application. In this work, the AgCl layer thickness was increased via a different choice of anodization, i.e., increasing the current density. A thicker AgCl layer would potentially result in increased service life of the sensor. Anodization at high current densities (as sensors C and D in this work), however, was found to reduce the adhesion of the AgCl layer to the Ag substrate, along with increase in impurities and AgCl

layer restructuring. These points were discussed in detail in "Correlation of sensors' response, surface properties and ohmic resistance of AgCl" section. The weak adhesion, increased heterogeneity and interfacial de-bonding in these cases will ultimately bring a sensor failure during practical use. The presence of impurities is not only a limitation for the long-term performance of the sensor in highly alkaline medium, but will also result in an inaccurate response. This would be of significant importance when interference of hydroxide ions in the medium (as in alkaline environment of nonsignificant chloride content) is at hand, resulting in transformation of AgCl to silver oxide. Increasing the chloride content in the medium, would lead to a subsequent transformation of the oxides to AgCl, i.e., a Ag/AgCl sensor is reversible, an aspect which is as generally observed and fundamentally justified. However, the presence of impurities in the AgCl layer, i.e., a decreased amount of the AgCl as such, can be a limitation to reversibility. Hence, the fabrication of Ag/AgCl sensors needs careful considerations, specifically for application in cement-based systems (or alkaline medium in general). Considering the results in this paper on microstructural properties, electrochemical response and surface chemistry, this work can be considered as a contribution to a decision-making process for sensor's preparation, in view of the above-outlined aspects, and/or potential restrictions to sensors performance in alkaline medium.

Conclusions

The mechanism of formation of a AgCl layer on a Ag substrate was evaluated through cyclic voltammetry and potentiodynamic polarization of Ag in 0.1 M HCl. In view of Ag/AgCl sensors preparation, anodization of Ag wires was performed in identical medium (0.1 M HCl) and at four different current densities (0.5, 1, 2 and 4 mA/cm^2). The electrochemical response of the sensors to pre-defined chloride content in alkaline medium was recorded. ESEM observation and XPS analysis were performed and the relevant mechanisms on the development of surface morphology and resulting surface chemistry were discussed. A correlation was made on the results for sensors' response, microstructural properties and ohmic resistance of the obtained AgCl

layers. The following main conclusions can be summarized:

- The AgCl layer morphology, microstructure and surface chemistry depend on the anodization regime. Current density above 2 mA/cm^2 was found to increase the thickness, heterogeneity and the ionic resistivity of the AgCl layer. Silver oxide-based or carbon-based impurities were present on the surface of the sensor in amounts proportional to the thickness and heterogeneity of the AgCl layer.

- The overpotential for the working electrodes (the sensors) during anodization was found to be current-density dependent as well. At low current density regimes (e.g., 0.5 mA/cm^2), the overpotential increased linearly with time of anodization. In this condition, "packed-piled" AgCl particles are formed uniformly on the Ag substrate. At high current density (e.g., 4 mA/cm^2), when the increase in overpotential with time is nonlinear, a thicker and complex, bi-layer structure of AgCl will form. In this condition, the outer AgCl layer consists of "twisted" particles, inner gap-separated from small metallic Ag(AgCl) grains in the vicinity of the Ag substrate.

- Small (Ag)AgCl grains seemed to be embedded in the AgCl layer as well, judged from the microstructural analysis, surface chemistry results and the mechanisms involved during anodization (altered electrochemical state of the Ag substrate in conditions of recorded overpotential, higher than 2 V). The appearance of these inclusions leads to increase in ionic resistivity, nonproportional to the AgCl layer thickness, together with weakened adhesion of the AgCl layer to the Ag substrate.

- The microstructural analysis of the AgCl layers, coupled with surface chemistry assessment and altered ionic resistivity, justified the reasons behind alterations in the electrochemical response of the Ag/AgCl sensors in alkaline medium. This difference in the sensors' response is attributable to the variation in properties of the Ag/AgCl interface, which was a consequence of the different current levels during Ag anodization.

- The results in this paper contribute to the decision-making process of sensors' preparation, although long-term performance at varying

thickness of the AgCl layer is necessary to be studied in order to reach a decision on practical application. Ag/AgCl sensors, produced at low current densities (e.g., 0.5 mA/cm^2) were found to be of superior performance, compared to sensors, prepared at high current densities (e.g., 4 mA/cm^2). The produced AgCl layer at low current density is more uniform, homogeneous and compact, resulting in a stable response of the sensors in the model (aqueous) alkaline medium. These results need to be considered when an optimized production process is to be defined for the long-term, practical use of Ag/AgCl sensors.

Acknowledgements

Compliance with ethical standards

Conflicts of interest   The authors declare no conflict of interest.

References

[1] Elsener B, Zimmermann L, Bohni H (2003) Non-destructive determination of the free chloride content in cement based materials. Mater Corros 54(6):440–446

[2] Neuman MR (2000) Biopotential electrodes. The biomedical engineering handbook. Chapter 8, CRC Press LLC, Boca Raton

[3] Gao X, ZhanG J, YanG Y, Lu S (2011) Preparation of chloride ion selective electrode and its potential response to different chloride solutions representing concrete environments. Mater Sci Forum (Zürich-Stafa: Trans Tech Publ) 1206(675):537–541

[4] Bozzini B, Giovannelli G, Mele C (2007) Electrochemical dynamics and structure of the Ag/AgCl interface in chloride-containing aqueous solutions. Surf Coat Technol 201(8):4619–4627

[5] Lal H, Thirsk HR, Wynne-Jones WFK (1951) A study of the behaviour of polarized electrodes. Part I. The silver/silver halide system. Trans Faraday Soc 47:70–77

[6] Katan T, Gu H, Bennion DN (1976) Analysis of porous electrodes with sparingly soluble reactants IV. Application to Particulate Bed Electrode: Ag/AgCl System. J Electrochem Soc 123(9):1370–1376

[7] Jaya S, Rao TP, Rao GP (1987) Mono-and multilayer formation studies of silver chloride on silver electrodes from chloride-containing solutions. J Appl Electrochem 17(3):635–640

[8] Beck TR, Rice DE (1984) Conductivity of anodic silver chloride during formation. J Electrochem Soc 131(1):89–93

[9] Burstein GT, Misra RDK (1983) Electrochemistry of scratched silver electrodes in chloride solutions. Electrochim Acta 28(3):363–369

[10] Birss VI, Smith CK (1987) The anodic behavior of silver in chloride solutions—I. The formation and reduction of thin silver chloride films. Electrochim Acta 32(2):259–268

[11] Jin X, Lu J, Liu P, Tong H (2003) The electrochemical formation and reduction of a thick AgCl deposition layer on a silver substrate. J Electroanal Chem 542:85–96

[12] Ha H, Payer J (2011) The effect of silver chloride formation on the kinetics of silver dissolution in chloride solution. Electrochim Acta 56(7):2781–2791

[13] Polk BJ, Stelzenmuller A, Mijares G, MacCrehan W, Gaitan M (2006) Ag/AgCl microelectrodes with improved stability for microfluidics. Sens Actuators B: Chem 114(1):239–247

[14] Shinwari MW, Zhitomirsky D, Deen IA, Selvaganapathy PR, Deen MJ, Landheer D (2010) Microfabricated reference electrodes and their biosensing applications. Sensors 10(3):1679–1715

[15] Shi X, Ye Z, Muthumani A, Zhang Y, Dante JF, Yu H (2015) A corrosion monitoring system for existing reinforced concrete structures (No. FHWA-OR-RD-15-14), Chicago

[16] Climent-Llorca MA, Viqueira-Perez E, Lopez-Atalaya MM (1996) Embeddable Ag/AgCl sensors for in situ monitoring chloride contents in concrete. Cem Concr Res 26(8):1157–1161

[17] Montemor MF, Alves JH, Simoes AM, Fernandes JCS, Lourenço Z, Costa AJS, Appleton AJ, Ferreira MGS (2006) Multiprobe chloride sensor for in situ monitoring of reinforced concrete structures. Cement Concr Compos 28(3):233–236

[18] Jin M, Jiang L, Zhu Q (2017) Monitoring chloride ion penetration in concrete with different mineral admixtures

based on embedded chloride ion selective electrodes. Constr Build Mater 143:1–15

[19] Atkins CP, Carter MA, Scantlebury JD (2001) Sources of error in using silver/silver chloride electrodes to monitor chloride activity in concrete. Cem Concr Res 31(8):1207–1211

[20] Stoica D, Brewer PJ, Brown RJ, Fisicaro P (2011) Influence of fabrication procedure on the electrochemical performance of Ag/AgCl reference electrodes. Electrochim Acta 56(27):10009–10015

[21] Brewer PJ, Leach AS, Brown RJC (2015) The role of the electrolyte in the fabrication of Ag|AgCl reference electrodes for pH measurement. Electrochim Acta 161:80–83

[22] Suzuki H, Hiratsuka A, Sasaki S, Karube I (1998) Problems associated with the thin-film Ag/AgCl reference electrode and a novel structure with improved durability. Sens Actuators B Chem 46(2):104–113

[23] Brewer PJ, Brown RJ (2010) Effect of silver annealing conditions on the performance of electrolytic silver/silver chloride electrodes used in Harned cell measurements of pH. Sensors 10(3):2202–2216

[24] Dobos D (1975) Electrochemical data: a handbook for electrochemists in industry and universities. Elsevier, Amsterdam

[25] Pargar F, Koleva DA, Kolev H, van Breugel K (2017) Determination of chloride content in cementitious materials: from fundamental aspects to application of Ag/AgCl chloride sensors. Sensors 17(11):2482

[26] Koleva DA, Boshkov N, Van Breugel K, De Wit JHW (2011) Steel corrosion resistance in model solutions, containing waste materials. Electrochim Acta 58(1):628–646

[27] Koleva DA, Denkova AG, Boshkov N, Van Breugel K (2013) Electrochemical performance of steel in cement extract and bulk matrix properties of cement paste in the presence of Pluronic 123 micelles. J Mater Sci 48(6):2490–2503. https://doi.org/10.1007/s10853-012-7037-3

[28] Shirley DA (1972) High-resolution X-ray photoemission spectrum of the valence bands of gold. Phys Rev B 5(12):4709–4714

[29] Scofield JH (1976) Hartree-Slater subshell photoionization cross-sections at 1254 and 1487 eV. J Electron Spectrosc Relat Phenom 8(2):129–137

[30] De Mele MFL, Salvarezza RC, Moll VV, Videla HA, Arvia AJ (1986) Kinetics and mechanism of silver chloride electroformation during the localized electrodissolution of silver in solutions containing sodium chloride. J Electrochem Soc 133(4):746–752

[31] Hills GJ, Schiffrin DJ, Thompson J (1974) Electrochemical nucleation from molten salts—I. Diffusion controlled electrodeposition of silver from alkali molten nitrates. Electrochim Acta 19(11):657–670

[32] Fletcher S (1983) Some formulae describing spherical and hemispherical diffusion to small crystals in unstirred solutions. J Cryst Growth 62(3):505–512

[33] Pritzker MD (1988) Voltammetric response for the diffusion-controlled electrodeposition onto growing hemispherical nuclei. J Electroanal Chem Interfacial Electrochem 243(1):57–80

[34] Isaev VA, Grishenkova OV (2013) Galvanostatic nucleation and growth under diffusion control. J Solid State Electrochem 17(6):1505–1508

[35] Fleischmann MTHR, Thirsk HR (1959) The potentiostatic study of the growth of deposits on electrodes. Electrochim Acta 1(2–3):146–160

[36] Giles RD (1970) The anodic behaviour of silver single crystal electrodes in concentrated chloride solutions. J Electroanal Chem Interfacial Electrochem 27(1):11–19

[37] Tilak BV, Perkins RS, Kozlowska HA, Conway BE (1972) Impedance and formation characteristics of electrolytically generated silver oxides—I formation and reduction of surface oxides and the role of dissolution processes. Electrochim Acta 17(8):1447–1469

[38] Burstein GT, Newman RC (1980) Anodic behaviour of scratched silver electrodes in alkaline solution. Electrochim Acta 25(8):1009–1013

[39] Fletcher S, Halliday CS, Gates D, Westcott M, Lwin T, Nelson G (1983) The response of some nucleation/growth processes to triangular scans of potential. J Electroanal Chem Interfacial Electrochem 159(2):267–285

[40] Boxall LG, Jones HL, Osteryoung RA (1974) Electrochemical studies on Ag, Fe, and Cu species in AlCl$_3$–NaCl melts. J Electrochem Soc 121(2):212–219

[41] Tuschel DD, Pemberton JE, Cook JE (1986) SERS and SEM of roughened silver electrode surfaces formed by controlled oxidation-reduction in aqueous chloride media. Langmuir 2(4):380–388

[42] Jovic BM, Jović VD, Dražić DM (1995) Kinetics of chloride ion adsorption and the mechanism of AgCl layer formation on the (111), (100) and (110) faces of silver. J Electroanal Chem 399(1–2):197–206

[43] Spangenberg A, Fleig J, Maier J (2001) Electromechanical writing on silver ion conductors. Adv Mater 13(19):1466–1468

[44] Evans JF, Albrecht MG, Ullevig DM, Hexter RM (1980) The physical and chemical characterization of electrochemically reformed silver surfaces. J Electroanal Chem Interfacial Electrochem 106:209–234

[45] Vera G, Climent MA, Anton C, Hidalgo A, Andrade C (2010) Determination of the selectivity coefficient of a

chloride ion selective electrode in alkaline media simulating the cement paste pore solution. J Electroanal Chem 639(1–2):43–49

[46] Svegl F, Kalcher K, Grosse-Eschedor YJ, Balonis M, Bobrowski A (2006) Detection of chlorides in pore water of cement based materials by potentiometric sensors. J Rare Metal Mater Eng 35(3):232–237

[47] Kaushik VK (1991) XPS core level spectra and Auger parameters for some silver compounds. J Electron Spectrosc Relat Phenom 56(3):273–277

[48] Ferraria AM, Carapeto AP, Botelho Do Rego AM (2012) X-ray photoelectron spectroscopy: silver salts revisited. Vacuum 86(12):1988–1991

[49] Wagner CD (1975) Chemical shifts of auger lines, and the auger parameter, faraday discuss. Chem Soc 60:291–300

[50] Hatsukade T, Kuhl KP, Cave ER, Abram DN, Jaramillo TF (2014) Insights into the electrocatalytic reduction of CO_2 on metallic silver surfaces. Phys Chem Chem Phys 16(27):13814–13819

[51] Gu H, Bennio DN (1977) Diffusion and charge transfer parameters for the Ag/AgCl electrode. J Electrochem Soc 124(9):1364–1370

[52] Pemberton JE, Girand MM (1987) Electrochemical and SEM characterization of Ag electrodes roughened by potential sweep and potential step processes in aqueous chloride and chloride + pyridine media. J Electroanal Chem Interfacial Electrochem 217(1):79–92

[53] Baetzold RC, Eachus RS (1995) The possibility of a split interstitial silver ion in AgCl. J Phys: Condens Matter 7(21):3991–3999

[54] Cain LS, Slifkin LM (1980) Ionic conductivity of mixed silver halide crystals. J Phys Chem Solids 41(2):173–178

[55] Altukhov VK, Shatalov VG (1987) Kinetics of silver oxidation and passivation in chloride solutions. Elektrokhimiya (Electrochemistry) 23(7):912–915

[56] Welham NJ, Kelsall GH, Diaz MA (1993) Thermodynamics of Ag–Cl–H_2O, Ag–Br–H_2O and Ag–I–H_2O systems at 298 K. J Electroanal Chem 361(1–2):39–47

[57] Kolodziej B (2000) The anodic behavior of silver in concentrated chloride solutions. Pol J Chem 74(3):349–360

[58] Brolo AG, Sharma SD (2003) Using probe beam deflection (PBD) to investigate the electrochemical oxidation of silver in perchlorate media in the presence and absence of chloride ions. Electrochim Acta 48(10):1375–1384

[59] Suzuki H, Taura T (2001) Thin-film Ag/AgCl structure and operational modes to realize long-term storage. J Electrochem Soc 148(12):E468–E474